ACS APPLIED ENERGY MATERIALS
Cite This: ACS Appl. Energy Mater. 2018, 1, 6136–6151
Article
www.acsaem.org

Influence of External Electric Fields on Photoluminescence and Charge Carrier Dynamics of π-Conjugated Polymer P3HT in Multilayer Films with Heterojunctions to TiO_2 and Sb_2S_3

Toshifumi Iimori,[†] Kamlesh Awasthi,[‡] Chin-Shiun Chiou,[‡] Eric Wei-Guang Diau,[‡,§] and Nobuhiro Ohta*[,‡,§]

[†]Department of Applied Chemistry, Muroran Institute of Technology, Mizumoto-cho, Muroran 050-8585, Japan
[‡]Department of Applied Chemistry and Institute of Molecular Science, National Chiao Tung University, 1001 Ta-Hsueh Road, Hsinchu 30010, Taiwan
[§]Center for Emergent Functional Matter Science, National Chiao Tung University, 1001 Ta-Hsueh Road, Hsinchu 30010, Taiwan

Supporting Information

ABSTRACT: π-conjugated polymers are actively studied as a promising component for developing inexpensive dye-sensitized solar cells (DSSCs). DSSCs utilizing π-conjugated polymers as p-type organic semiconductor and metal chalcogenides as sensitizers have attracted interest due to high absorbance and stability in comparison to DSSCs using conventional molecular dyes. Here, we report the study of the excited state and charge carrier dynamics in poly(hexylthiophene) (P3HT) with junction structures of FTO/TiO_2/P3HT/PMMA/Ag and FTO/TiO_2/Sb_2S_3/P3HT/PMMA/Ag, where fluorine-doped tin oxide (FTO) and silver (Ag) are used as electrodes and poly(methyl methacrylate) (PMMA) is used as an insulating film. We measured electroabsorption spectra and the effects of external electric fields on photoluminescence (PL) of P3HT in these two different systems. Two PL bands emitted from different emitting states are observed in both of the systems. As the quadratic electric field effect, fluorescence quantum yield and lifetime become larger and longer in both of the PL bands, respectively, in the presence of external electric fields, indicating that nonradiative decay processes are depressed by applied electric fields in both of the systems. We also measured the linear electric field effects on PL of P3HT, and PL enhancement and quenching of PL intensity as well as lengthening and shortening of PL lifetime were observed, depending on the direction of the applied electric fields. It is shown that the mechanism of the linear field effect is different between the two emitting states in both of the systems; i.e., the population of the emitting state is affected by application of electric field for one PL band but not for the other PL band. The anisotropy of the field-induced change in PL with respect to the field direction of the applied electric fields can be explained in terms of the synergy effect between internal electric field which exists in the P3HT film and externally applied electric field on the charge separation of hot excitons generated following photoexcitation to free electron and hole (polaron) and on nonradiative decay rate of the PL emitting states.

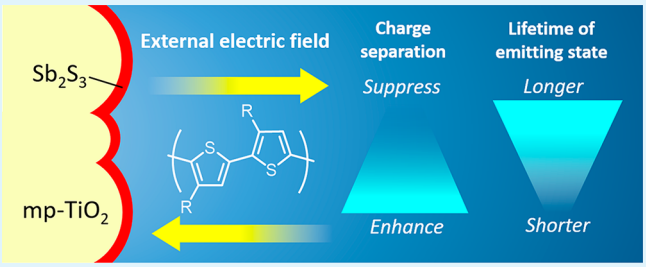

KEYWORDS: *dye-sensitized solar cell, conjugated polymer, stark effect, photoexcitation dynamics, electrophotoluminescence spectrum, time-resolved emission decay*

INTRODUCTION

Solar cells utilizing π-conjugated polymers are attracting special attention because of promising performance as inexpensive renewable energy sources.[1−5] Solar cells utilizing π-conjugated polymers are classified into two categories of organic thin film solar cell and dye-sensitized solar cell (DSSC). As an example of the former device, bulk heterojunction solar cells obtained by blending π-conjugated polymers with phenyl-C_{61}-butylic acid methyl ester (PCBM) put a high impact on the field of organic solar cell due to simple preparation and good conversion efficiency.[6] On the other hand, serious effort is still put into improving the performance of the latter DSSC.[7−11] The sensitization of wide-gap semiconductor, such as TiO_2, with dyes absorbing visible or near-infrared light is a principle of the structure of DSSC, and a hole transport layer is also a component of DSSC.

Recently, inorganic materials have been attracting growing interest as the alternatives to conventional organic dyes for the sensitizers.[12−17] The use of inorganic sensitizers has some advantages including high extinction coefficient, spectral

Received: July 17, 2018
Accepted: September 28, 2018
Published: October 15, 2018

DOI: 10.1021/acsaem.8b01171
ACS Appl. Energy Mater. 2018, 1, 6136–6151

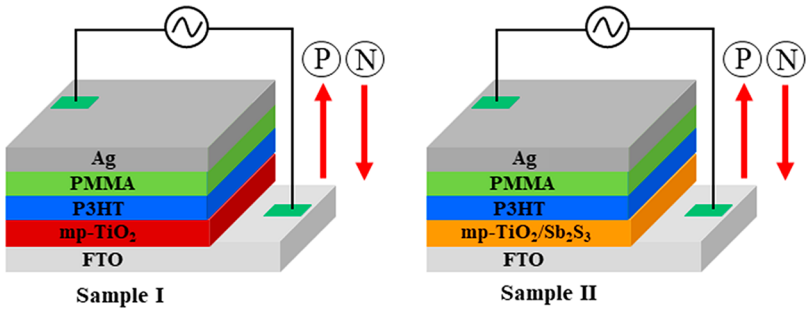

Figure 1. Layer structure of the devices used for the electroabsorption (E-A) and E-PL measurements. Positive and negative field directions used in the text are shown by the red arrows indicated by P and N, respectively.

tunability, good stability, and multiple exciton generation.[18−24] Antimony sulfide (Sb_2S_3), which is metal chalcogenide, is one of the most promising materials due to high optical extinction coefficient and narrow band gap of 1.7 eV, which is suitable for visible light absorption.[25] The inorganic/organic heterojunction solar cell having the interface of TiO_2/Sb_2S_3 forms a type-II staggered heterostructure, and the energy levels among TiO_2, Sb_2S_3, and poly(hexylthiphene) (P3HT) in a hole transport layer are matching for photovoltaic application (Figure S1 of the Supporting Information (SI)).[26,27] For the DSSC with the structure of Sb_2S_3/P3HT, a high efficiency of 5.1% has been reported,[28] which is higher than that of the heterojunction cell of Sb_2S_3/CuSCN.[24] In these cells, the electrons generated by the photoexcitation of Sb_2S_3 are injected to the mesoporous (mp-) TiO_2 layer, and the holes are transported to the P3HT layer.

The photoabsorption also occurs in the P3HT layer and generates charge carriers. It is possible that the electrons generated in the P3HT layer are transferred to the mp-TiO_2 or Sb_2S_3, and the generated holes can be transferred to the counter electrode opposite to the FTO electrode. However, the charge recombination of the hole−electron pairs produced by photoexcitation of P3HT may occur in the P3HT layer, and this process may disturb the hole transport from Sb_2S_3 and induce the depression of external quantum efficiency. It is noted that the incident-photon-to-current efficiency (IPCE) of the cell with the TiO_2/P3HT structure without Sb_2S_3 is smaller than 5% at 500 nm. The overall conversion efficiency was 0.092%, suggesting insufficient charge generation and transfer at the TiO_2/P3HT interface, and the Sb_2S_3 layer plays an important role for increasing the efficiency of DSSC. Therefore, the comparison of carrier dynamics in P3HT for the DSSCs with TiO_2/P3HT and TiO_2/Sb_2S_3/P3HT structures are of importance toward the understanding of factors controlling carrier dynamics in the DSSC.

Investigation of the external electric field effects on photoluminescence (PL) is extremely useful for the understanding of dynamics of photogenerated carriers in π-conjugated polymers. The energy level of charge carriers can be greatly perturbed with the application of external electric fields. Since the kinetics of the photoinduced charge carriers can be monitored through the PL lifetime, we can expect to obtain information on carrier kinetics from electric field-induced change in PL intensity as well as PL lifetime. In a bare P3HT film without heterojunction structure, photoexcitation can produce photocarriers. The PL quantum yield (QY) of P3HT in the form of solid film is very small (0.02) in contrast with that in solution (0.33).[29] Transient absorption spectroscopic study revealed that this reduction of the QY results from the efficient polaron formation after photoexcitation.[29] Time-resolved study of the field-induced fluorescence quenching was also measured for poly(phenylphenylenevinylene) (PPV), showing that the photocarriers are generated from the dissociation of exciton.[30] The measurements of the electrophotoluminescence (E-PL) spectra, i.e., electric field effect on PL spectra, are also useful to obtain valuable information on the carrier dynamics. For sulfide-substituted PPV derivative, the efficiency of field-induced quenching depends on the photoexcitation energy, suggesting that the efficiency of field-assisted generation of electron−hole pairs from the exciton increased with the increase in photoexcitation energy.[31]

Issues on internal electric fields originating from a build-in potential at heterojunctions are also of emerging interest, because they may affect overall efficiency of DSSC.[32,33] The investigation of E-PL as a result of the perturbation of external electric fields allows us to gain insight into the internal electric fields in DSSC. In fact, for a methylammonium lead iodide perovskite film, the presence of strong internal fields was suggested from the measurements of steady-state and time-resolved E-PL measurements.[34]

In the present study, carrier dynamics of P3HT in the cells with multilayer structures that are relevant to DSSC is discussed. The cells investigated here have different junctions of FTO/TiO_2/Sb_2S_3/P3HT/PMMA/Ag and FTO/TiO_2/P3HT/PMMA/Ag, where the definitions of the abbreviations will be given in the next section, Experimental Methods. In general, Stark spectroscopy including E-PL measurements detects the signal at the second harmonic of the modulation frequency of applied electric fields. We can deduce the second-order Stark effect from this type of conventional experiments.[35,36] Further, we employed the first harmonic detection of the modulated electric field with the aim to obtain insight into anisotropic dynamics existing in the cell, in addition to the quadratic field effect. By changing the polarity of the electrodes of FTO and Ag, we changed the direction of the applied electric field on the cell and extracted anisotropic response which depends on the direction of applied electric fields. We have made not only steady-state E-PL measurements but also time-resolved E-PL measurements, and field-direction dependence of PL as well as excitation dynamics has been examined.

EXPERIMENTAL METHODS

Sample Preparation. Poly(methyl methacrylate), denoted as PMMA (Aldrich, averaged MW = 120000) was purified by precipitation with a mixture of benzene and methanol and by extraction with hot methanol. As shown in Figure 1, two types of film, i.e., FTO/mp-TiO_2/P3HT/PMMA/Ag (sample I) and FTO/mp-TiO_2/Sb_2S_3/P3HT/PMMA/Ag (sample II) were studied in this

DOI: 10.1021/acsaem.8b01171
ACS Appl. Energy Mater. 2018, 1, 6136−6151

work, where FTO and mp-TiO_2 represent a fluorine-doped tin oxide-coated glass substrate and a mesoporous TiO_2 film, respectively. Detailed layer structure will be discussed later, based on the measurements of field-induced scanning electron microscope (SEM) images.

A schematic diagram of sample preparation is shown in Figure S2 of the SI. A certain area of FTO substrate (Sinonar) was etched by using zinc powder and HCl solution (4N), and washed with detergent, water/acetone/isopropanol mixture, and deionized water, and then cleaned with an ultraviolet−ozone cleaner for 18 min. mp-TiO_2 films were fabricated on the FTO substrate with the spin coating of TiO_2 paste (Degussa P25, average diameter of 50 nm) and sintered in an oven at 500 °C. Thickness of the TiO_2 film was ca. 200 nm. In a typical synthesis of Sb_2S_3, a chemical bath solution was prepared by dissolving 2.6 g of $SbCl_3$ in 10 mL of acetone and subsequently by adding 100 mL of 1 M $Na_2S_2O_3$ solution and 290 mL of deionized water. For the deposition of Sb_2S_3, the FTO substrate coated with the mp-TiO_2 film was placed vertically along the wall of a beaker containing the bath. After the formation of an orange film, the substrate was taken out from the bath, washed well with deionized water, and dried in an oven. Subsequently, a final deposition of Sb_2S_3 was done at 4 °C for 180 min in the bath placed inside a temperature-controlled refrigerator. In order to obtain brown crystalline Sb_2S_3, the substrate was annealed under nitrogen for 30 min at 300 °C. After the annealing, the substrate was stored in dry air until further characterization. After the characterization of the mp-TiO_2−Sb_2S_3 film, we deposited P3HT solution on the substrate by using spin coating technique. The P3HT solution was prepared by dissolving regioregular P3HT (MW = 15000−45000, Rieke metals) of 15 mg in 1 mL of chlorobenzene. We then deposited PMMA film on the P3HT film by using spin-coating technique with PMMA solution (0.4 g in 10 mL of benzene). Then, a semitransparent silver film was deposited on the PMMA film by using vacuum vapor deposition technique. The FTO and Ag films were used as electrodes. Sample I and sample II without and with Sb_2S_3 on mp-TiO_2 layers, respectively, were prepared by similar procedures.

Sample Characterization. SEM (SU8010, Hitachi) was used to take images of the mp-TiO_2 film before and after the deposition of Sb_2S_3 (Figure 2). We could see the difference between the films with

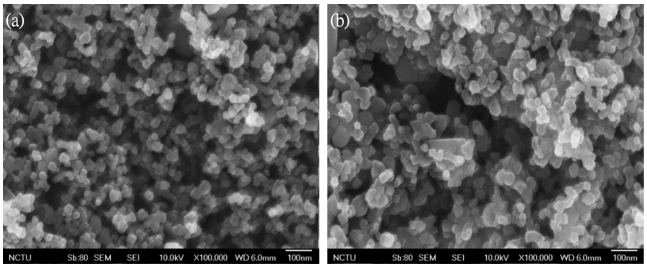

Figure 2. SEM image of (a) the pristine mp-TiO_2 film and (b) the mp-TiO_2 film after the chemical bath deposition of Sb_2S_3.

and without Sb_2S_3.[27] Before the deposition of Sb_2S_3 (Figure 2a), we found a number of pores among TiO_2 nanoparticles, indicating that nanoparticles of TiO_2 presented an easily accessed open structure for Sb_2S_3 deposition. Due to the chemical deposition of Sb_2S_3, the particle size increased and the porosity of the film decreased, as shown in Figure 2b. Then, the layer composed of mp-TiO_2 and Sb_2S_3 was regarded as a mixture of mp-TiO_2 and Sb_2S_3, with a thickness of ∼200 nm.

The cross-sectional SEM image of FTO/mp-TiO_2/P3HT/PMMA, which corresponds to sample I, was also observed. The results are shown in Figure 3. The P3HT film cannot be identified well, so it is not clear whether P3HT is penetrated into mp-TiO_2 film or not. However, it is unlikely that P3HT penetrates into the mp-TiO_2 or mp-TiO_2/Sb_2S_3 layer because of the nonpolarity of the solvent used for the spin-coating of P3HT. From the SEM image of P3HT coated on FTO with a similar absorbance, the thickness of P3HT film may be

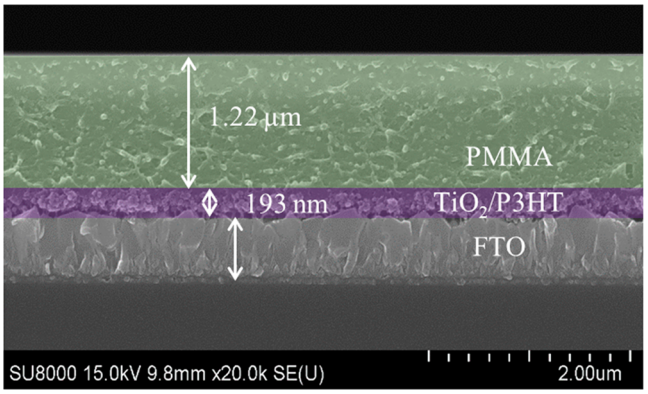

Figure 3. SEM image of the layer structure of FTO/mp-TiO_2/P3HT/PMMA.

roughly estimated to be 20 nm, if P3HT is not penetrated into the mp-TiO_2 film. The thickness between the surface of FTO and the top layer of PMMA was measured by using a surface roughness meter (Veeco Dektak 150). This thickness, which was under a decisive necessity for the electroabsorption (E-A) and E-PL measurements, was 1.0 ± 0.4 μm, depending on the sample. Silver films were finally deposited with a thickness in the range of 25−30 nm.

Electroabsorption and Electro-photoluminescence Measurements. All the measurements were carried out at room temperature. Absorption spectra were obtained with a commercial instrument (JASCO, V-570). Steady-state electroabsorption measurements were done with a commercial spectrometer (EMV-100, JASCO), the detail of which was reported elsewhere.[37−39] Sinusoidal alternating current (AC) voltage of 1 kHz, which was generated by a function generator (SG-4311, Iwatsu) and amplified by a high voltage amplifier, was applied between the electrodes of substrates. Field-induced change in intensity of the linearly polarized light transmitted through the substrate was detected with a lock-in amplifier (Stanford Research System, SR830) at the second harmonic of the modulation frequency. Direct current component (DC) of the transmitted light intensity was simultaneously monitored. The change in absorption intensity (ΔA) was determined from the field-induced change and DC component of the transmitted light intensity. E-A spectra were obtained by plotting ΔA as a function of wavelength, and the spectra were converted to the ones as a function of wavenumber by the conventional way. The angle between the direction of the applied electric field and the electric vector of the excitation light was set to be 54.7° in the E-A measurements. Applied field strength was evaluated from the applied voltage divided by the distance between two electrodes.

E-PL spectra corresponds to the field-induced change in PL spectra. The PL intensity at zero field and its field-induced change are hereafter represented by I_{PL} and $\Delta I_{PL} = I_{PL}(F\neq 0) - I_{PL}(F=0)$, respectively. E-PL spectra represent the plots of ΔI_{PL} as a function of wavenumber. E-PL spectra were measured with a spectrofluorometer (JASCO, FP777) combined with a lock-in amplifier.[39] In the present study, E-PL spectra were obtained with excitation at wavelengths at which field-induced change in absorption intensity was negligibly small. The sample substrate was kept under vacuum, and the incident angle of the light on the substrate was 45°. The frequency of the applied AC voltage was 40 Hz in the E-PL measurements. The field-induced change in PL intensity was detected by a lock-in amplifier, not only at the second harmonic but also at the first harmonic of the modulation frequency. It was confirmed that emission was negligible for the sample having a layer structure of FTO/mp-TiO_2/Sb_2S_3/PMMA/Ag. Therefore, the PL observed in the present study is attributed only to P3HT.

In addition to the steady-state E-PL measurements, we carried out time-resolved E-PL decay measurements with the system reported elsewhere.[34,40] The experimental procedure is described in the SI (Figure S3).

DOI: 10.1021/acsaem.8b01171
ACS Appl. Energy Mater. 2018, 1, 6136−6151

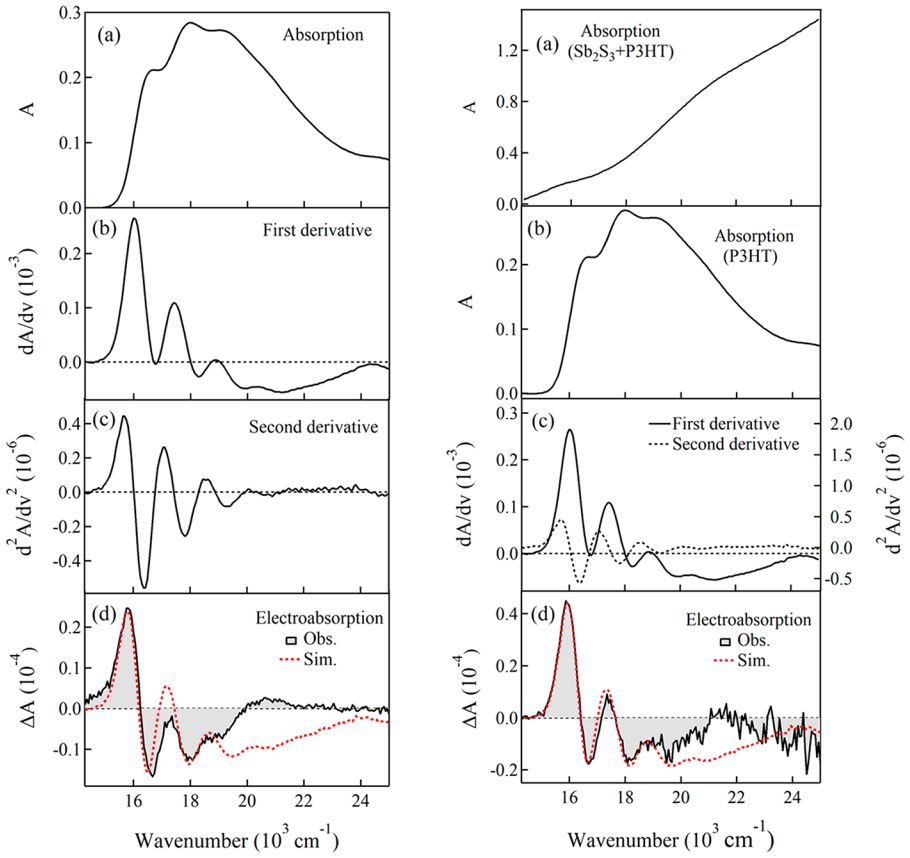

Figure 4. (Left) Absorption spectrum (a), the first and second derivatives of the absorption spectrum (b, c), and the E-A spectrum (d) of sample I (FTO/mp-TiO_2/P3HT/PMMA/Ag), and (right) absorption spectrum of sample II (FTO/mp-TiO_2/Sb_2S_3/P3HT/PMMA/Ag) (a), absorption spectrum of P3HT used for the simulation (b), the first and second derivatives of the absorption spectrum of P3HT (c), and the E-A spectrum of sample II (d). The applied field strength was 0.3 MV cm^{-1} in both cases. In panel d, the black solid line is the observed E-A spectrum, and the red broken line is the simulated spectrum using eq 1. The absorption spectrum of sample I was used for the simulation of the E-A spectrum of sample II. See the text for the detail.

RESULTS

E-A Spectra. According to the theory of electric field effects on optical spectra,[35,36,39,41−43] field-induced change in absorbance for molecules can be expressed as a linear combination of the zeroth, first, and second derivatives of the absorption spectra:

$$\Delta A(\nu) = (fF)^2\left[A_\chi A(\nu) + B_\chi \nu \frac{d(A(\nu)/\nu)}{d\nu} + C_\chi \nu \frac{d^2(A(\nu)/\nu)}{d^2\nu}\right] \quad (1)$$

where ν is the wavenumber of light, $A(\nu)$ is the absorbance at ν, f is the internal field factor, F is the field strength, and A_χ, B_χ, and C_χ are the coefficients for the zeroth, first, and second derivatives of $A(\nu)$, respectively. We carried out the experiments at a magic angle condition of $\chi = 54.7°$, where χ is the angle between the external electric field, **F**, and polarization direction of the excitation light. Moreover, we can assume that molecules are isotropically distributed and immobilized in rigid matrices such as the P3HT film. In this case, the coefficient B_χ and C_χ are reduced to

$$B_\chi \cong \frac{\Delta\bar{\alpha}}{2hc} \quad (2)$$

$$C_\chi \cong \frac{|\Delta\mu|^2}{6h^2c^2} \quad (3)$$

In these equations, $\Delta\bar{\alpha}$ is the trace of the difference of the molecular polarizability tensor between the excited state and the ground state,

$$\Delta\bar{\alpha} = \frac{1}{3}\mathrm{Tr}(\alpha_e - \alpha_g) \quad (4)$$

and α_e and α_g are the molecular polarizabilities of the excited state and the ground state, respectively. $\Delta\boldsymbol{\mu}$ is the difference of the electric dipole moments between the excited state and the ground state,

$$\Delta\boldsymbol{\mu} = \mu_e - \mu_g \quad (5)$$

where μ_e and μ_g are the electric dipole moments of the excited state and the ground state, respectively. With these equations, we can calculate $\Delta\bar{\alpha}$ and $\Delta\boldsymbol{\mu}$ from the first and second derivative coefficients B_χ and C_χ in the E-A spectra, respectively. The zeroth derivative component A_χ may arise from the electric field-induced change in transition dipole moment.

Absorption and E-A spectra of samples I and II were measured. The results are shown in Figure 4. The magnitude of ΔA is proportional to the square of the applied field strength, as expected from eq 1 (Figure S4 of SI). We simulated the E-A spectrum with a sum of the zeroth, first, and second derivatives of the absorption spectrum, and the simulated spectrum is also shown in the figure. The Sb_2S_3

DOI: 10.1021/acsaem.8b01171
ACS Appl. Energy Mater. 2018, 1, 6136−6151

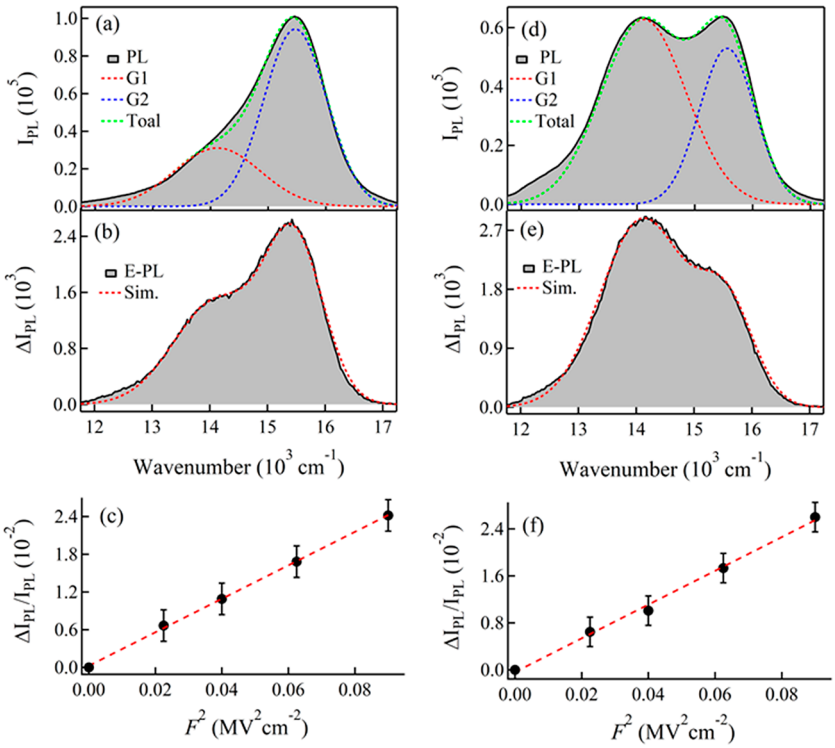

Figure 5. (a, d) PL spectra and their decomposition to the bands G1 (red dotted line) and G2 (blue dotted line) having a Gaussian profile, which were used for the simulation. (b, e) E-PL spectra (shaded line) at a field strength of 0.3 MV cm^{-1} and the simulated spectra (red dotted line). (c, f) Signal intensity of E-PL as a function of square of the applied field strength. The results of sample I and sample II are depicted in the left and right columns, respectively. G1 and G2 have maxima at 14049 and at 15458 cm^{-1}, respectively.

film which existed in sample II showed much larger absorbance than that of P3HT (cf. Figure 4a for samples I and II), and it was difficult to separate the observed absorption spectrum of sample II into each of the absorption spectra of P3HT and Sb_2S_3. On the basis of the E-A measurements of the sample having a layer structure of FTO/mp-TiO_2/Sb_2S_3/PMMA/Ag, the E-A signal of Sb_2S_3 film was confirmed to be negligibly small, indicating that the E-A spectrum of sample II resulted from P3HT. Therefore, we used the absorption spectrum of sample I in order to analyze the E-A spectra of sample II, by assuming that the absorption spectrum of P3HT was the same for the samples with and without Sb_2S_3 layer. In fact, the E-A spectra of both samples were very similar in shape to each other, as shown in Figure 4, which supports the above assumption.

It is worth mentioning that the coefficient A_χ is very small in any samples, i.e., ~3 × 10^{-4} and ~4 × 10^{-4} MV^{-2} cm^2, respectively, in samples I and II, indicating that the transition moment of the absorption band is little affected by **F**. The electric field effect on the molecular transition moment, i.e., the effect on the absorption coefficient, is small for allowed transitions, e.g., in π-conjugated polymers, and can therefore be neglected relative to the terms caused by the change in electric dipole moment and/or molecular polarizability following absorption.[30,31,44−47] The values of $\Delta\bar{\alpha}$ and $|\Delta\boldsymbol{\mu}|$ for the electronic transition of P3HT were determined using eqs 2 and 3, i.e., $f|\Delta\boldsymbol{\mu}|$ = 2.6 D, $f^2\Delta\bar{\alpha}$ = 28 $Å^2$ in sample I and $f|\Delta\boldsymbol{\mu}|$ = 2.9 D, $f^2\Delta\bar{\alpha}$ = 59 $Å^2$ in sample II, where f is the internal field factor. Sample II that has the structure of FTO/mp-TiO_2/Sb_2S_3/P3HT/PMMA/Ag exhibits larger values of both $\Delta\bar{\alpha}$ and $|\Delta\boldsymbol{\mu}|$ following transition to the photoexcited state. It is likely that the magnitude of $\boldsymbol{\alpha}_e$ and $\boldsymbol{\mu}_e$ in the excited state of P3HT is larger than that in the ground state. Then, the significant magnitude of $|\Delta\boldsymbol{\mu}|$ indicates the charge-transfer (CT) character of the photoexcited state. $\boldsymbol{\alpha}_e$ and $\boldsymbol{\mu}_e$ of P3HT that was coated on the Sb_2S_3 layer are slightly larger than those of the sample having no Sb_2S_3 layer, suggesting that the CT character of the photoexcited state of the P3HT film is a little enhanced when the Sb_2S_3/P3HT junction is formed. It is also mentioned that PL spectra of these samples are different from each other, as will be shown later. The enhancement of the CT character following photoexcitation may be explained by more efficient separation of hole and electron pairs in the exciton state at the Sb_2S_3/P3HT interface. A similar enhancement of E-A signal was reported for the interface between P3HT and PCBM, because of the formation of the charge-transfer complex.[48] In the present sample, there was no notable contribution of the charge-transfer complex to the E-A spectra, which may show a large value of $|\Delta\boldsymbol{\mu}|$, though the charge-transfer complex between Sb_2S_3 and P3HT may be formed at the Sb_2S_3/P3HT interface.

Similar E-A spectra for conjugated polymers including poly(thiophene) have been reported by some groups.[44,45,49,50] The principal feature in the E-A spectrum appearing in the range from 15000 to 19000 cm^{-1} was assigned to the Stark shift of the low-lying ^1B_u exciton state. The discrepancy of the simulation in the region above 19000 cm^{-1} was also recognized in the previous E-A studies, and the discrepancy was ascribed to the contribution of the optically forbidden mA_g exciton state which can mix with the ^1B_u state by the perturbation of electric fields.[45,50] As the origin of the discrepancy, another possibility may be considered that aggregated and amorphous forms which give different field effects from each other exist in the solid film of P3HT.

DOI: 10.1021/acsaem.8b01171
ACS Appl. Energy Mater. 2018, 1, 6136−6151

E-PL Spectroscopy. E-PL spectrum observed at the second harmonic of the modulation frequency is considered to be given by a combination of the zeroth, first, and second derivatives of the PL spectrum, which is similar to the E-A spectrum and eq 1. Both the first and second derivative components come from the second-order Stark effect on the PL band, as in the case of E-A spectra. In principle, the analysis of these components can afford the determination of $\Delta\bar{\alpha}$ and $|\Delta\boldsymbol{\mu}|$ between the emitting state and the ground state. In the present results, however, the coefficient of the zeroth derivative component is extremely large, so the first and second derivative components could not be determined. The zeroth derivative component shows the change in PL intensity induced by the applied electric field (ΔI_{PL}) relative to the unperturbed PL intensity (I_{PL}), thus giving information on the field-induced change in emission quantum yield.[39,51,52] Then, electric field effects on photoexcitation dynamics can be discussed, based on the zeroth derivative component of the E-PL spectrum.

E-PL spectra observed at the second harmonic of the modulation frequency of the applied AC voltage are shown in Figure 5. The PL and E-PL spectra were measured simultaneously with excitation wavelength at 450 nm with F = 0.3 MV cm^{-1}. At this excitation wavelength, the field-induced change in absorption intensity (i.e., ΔA) was so small that we could measure the E-PL spectra which did not include the contribution of the field-induced change in absorption intensity. We could reproduce the main feature of the PL spectra as well as E-PL spectra by using two Gaussian line shapes indicated by G1 and G2. The energy separation between the G1 and G2 bands is nearly ∼1300 cm^{-1} for the P3HT films. As far as this energy separation is concerned, G1 and G2 look like vibronic progression. If G1 and G2 originate from the same origin, the efficiency of the field-induced change in PL intensity, i.e., $\Delta I_{PL}/I_{PL}$ must be the same for G1 and G2. As shown later, however, the magnitude of the field-induced change in PL intensity is very different from each other for G1 and G2. Further, G1 and G2 show different decay profiles, indicating that G1 and G2 are emitted from different origins. Then, G1 and G2 are considered to be emitted from different electronic states of P3HT film. Brown et al. reported that the emission bands can be assigned to the sum of two different Franck−Condon series, probably coming from interchain and intrachain interactions.[53] Even so, it is likely that the G1 and G2 bands result from the exciton located near the interface and exciton located insider P3HT, respectively. The low-energy trap states of aggregated and amorphous forms of P3HT may correspond to these emitting states of G1 and G2. Spano and Silva suggested that features of PL spectra of P3HT can be explained in terms of weakly coupled H-aggregates of P3HT polymer chains.[54] Therefore, G1 and G2 bands may be emitted from a single state corresponding to the H-aggregates of P3HT. However, the facts that the ratio between G1 and G2 is different between samples I and II and that there is the difference in the field-induced change in the PL intensity suggest that the G1 and G2 bands are related to two different emitting states.

The spectral shapes of the E-PL spectra corresponding to G1 and G2 are similar to those of the PL spectra. In fact, the E-PL spectra could be simulated well only by the sum of the zeroth derivative components of these PL bands of G1 and G2. In both samples I and II, the integrated intensities of the E-PL spectra are positive, showing that the PL quantum yield increases in the presence of **F**. It is noted that the magnitude of $\Delta I_{PL}/I_{PL}$ is proportional to the square of the applied field strength, as shown in Figure 5. This result is consistent with the expectation that we must observe the second-order field effect on the PL intensity if we detect the signal at the second harmonic of the modulation frequency of the applied electric field.

The magnitudes of the field-induced change in the PL quantum yield for these two Gaussian PL bands were evaluated from $\Delta I_{PL}/I_{PL}$. The results are shown in Table 1, together with the intensity ratio between the G1 and G2 bands. PL intensity changes by 2−5% with a field strength of 0.3 MV cm^{-1}, indicating that the PL quantum yield increases by 2−5% in the presence of 0.3 MV cm^{-1} in these samples, as the quadratic field effect. Here, we have to note that photobleaching of PL occurs during the measurements of PL and E-PL spectra and that photobleaching is a little more efficient for the G2 band, which is located in the higher wavenumber region, than that for the G1 band. However, there is no doubt that the ratio between ΔI_{PL} and I_{PL} shown in Table 1 is reliable for both G1 and G2, since both PL and E-PL spectra were measured simultaneously in the present experiments.

Table 1. $\Delta I_{PL}/I_{PL}$ for G1 and G2 of Samples I and II Determined from the E-PL Spectra Observed at the Second Harmonic of the Modulation Frequency of F and PL Spectra Observed Simultaneously[a,b]

		$\Delta I_{PL}/I_{PL}$	
	$I_{PL}(G1)/I_{PL}(G2)$	G1 band	G2 band
sample I	0.352	0.040	0.024
sample II	1.21	0.046	0.028

[a]The applied field strength was 0.3 MVcm^{-1}. Note that ΔI_{PL} is proportional to the square of the magnitude of F. The ratio of the intensity between G1 and G2 which was obtained from the ratio of the peak intensity of the PL spectrum is also shown. [b]I_{PL} is the PL intensity. ΔI_{PL} is the field-induced change in I_{PL}.

E-PL spectra were also observed at the first harmonic of the modulation frequency; E-PL spectra were measured under two different directions of **F**, where positive electrode was connected to FTO and negative electrode was connected to silver, hereafter called positive field direction (Figure 1), and positive electrode was connected to silver and negative electrode was connected to FTO, called negative field direction (Figure 1). The results which are shown in Figures 6 and 7 for sample I and sample II, respectively, clearly show that the effect of **F** on the PL depends on the direction of **F**. In the positive field direction, the intensity of the E-PL spectrum was positive (Figures 6b and 7b), indicating the field-induced increase of the quantum yield of PL for both G1 and G2. In the negative field direction, on the contrary, the intensity of the E-PL spectrum is negative (Figures 6e and 7e), indicating the field-induced decrease of the quantum yield of PL for both G1 and G2. The magnitude of $\Delta I_{PL}/I_{PL}$ shows a linear field strength dependence (see Figures 6c,f and 7c,f), which confirms the linear field effect on PL. The coefficients of the zeroth derivative component, i.e., the values of $\Delta I_{PL}/I_{PL}$ for the G1 and G2 bands, are summarized in Table 2.

There is a difference in magnitude of $\Delta I_{PL}/I_{PL}$ between G1 and G2 (see Figures 6 and 7 and Tables 1 and 2), indicating that electric field effects on photoexcitation dynamics at the emitting states of these two bands are different from each other. The PL lifetimes monitored at these two bands are also

DOI: 10.1021/acsaem.8b01171
ACS Appl. Energy Mater. 2018, 1, 6136−6151

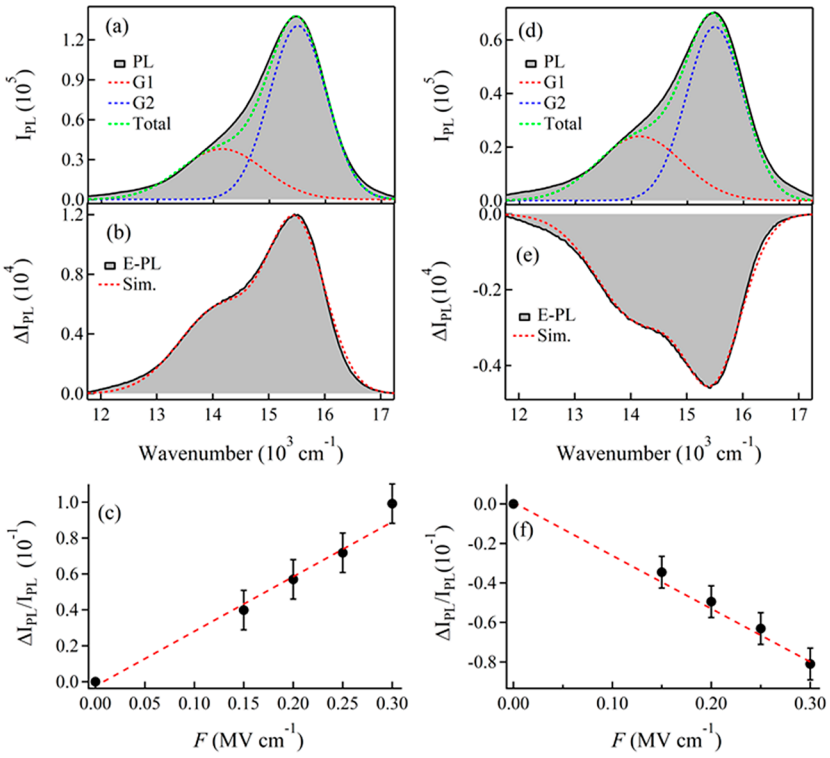

Figure 6. (a, d) PL spectra of sample I and its decomposition to the bands G1 and G2 having a Gaussian profile. (b, e) E-PL spectra observed with the first harmonic of the modulation frequency of the applied field having a strength of 0.3 MV cm^{-1} with positive direction (b) and negative direction (e) and the simulated E-PL spectra (red dotted line) as a sum of the G1 and G2 band. (c, f) Plots of $\Delta I_{PL}/I_{PL}$ as a function of the applied electric field strength. In the plots, the maximum intensity of G1 of the E-PL spectra was monitored. PL and E-PL spectra were simultaneously measured. The spectra observed with a field having the negative direction was measured following the measurements with a field having the positive direction.

different from each other, as shown later. These results indicate that the emitting states, from which the relaxation to the ground state occurs, are not a sole electronic state.

As the origin of the electric field effects on the PL intensity, that is, on the PL quantum yield, two possibilities can be pointed out: (1) field-induced change in the yield of population of the PL emitting state from the photoexcited Franck−Condon state; (2) field-induced change in radiative decay rate and/or nonradiative decay rate at the PL emitting state. Field-induced increase (decrease) of the population of the PL emitting state results in the increase (decrease) of the PL intensity. Field-induced decrease (increase) of nonradiative decay rate or field-induced increase (decrease) of the radiative decay rate also results in the increase (decrease) of the PL intensity. Understanding of detailed mechanisms is difficult solely from the steady-state measurements of the E-PL spectra. Hence, measurements of the field-induced change in PL decay profile were carried out.

Field-Induced Change in the PL Decay Profile. In order to examine the origin of the field-induced change in the PL intensity (emission quantum yield), we compared the PL decay profiles of P3HT observed in the absence and presence of **F** (0.3 MV cm^{-1}). The results are shown in Figures 8−11 and Figures S5−S8 of the SI for samples I and II. The PL decay curves were monitored at 640 and 705 nm, which corresponds to the intensity maxima for G2 and G1, respectively, with excitation at 450 nm. As explained in the SI (Figure S3), four memory segments of the multichannel analyzer store the fluorescence decay curves which correspond to the applied fields of +0.3, 0, −0.3, and 0 MV cm^{-1}, respectively. Hereafter, these decay curves are called CH1, CH2, CH3, and CH4, respectively. We simulated the decay curves at 0.3 MV cm^{-1} [$I(t)_{ON}$] and at zero field [$I(t)_{OFF}$]; that is, $I(t)_{ON}$ = CH1 + CH3, and $I(t)_{OFF}$ = CH2 + CH4. Note that the decay profiles which correspond to $I(t)_{ON}$, $I(t)_{OFF}$, $I(t)_{ON}$ — $I(t)_{OFF}$, and $I(t)_{ON}/I(t)_{OFF}$, respectively, are shown in Figures 8 and 9. $I(t)_{ON}$ gives the decay including only the quadratic field effect, since the linear filed effect which shows the opposite field-direction dependence is canceled to each other by adding CH1 and CH3, while $I(t)_{OFF}$ gives the decay at zero field.

Decay profiles of $I(t)_{ON}$ and $I(t)_{OFF}$ were simulated by assuming a triexponential decay, that is, $\sum_{i=1}^{3} A_i \exp(-t/\tau_i)$, where τ_i is the lifetime and A_i is the pre-exponential factor of the ith component. The difference in τ_i and A_i between the values in the presence and absence of **F** is very small, but we could determine these parameters by simultaneously simulating the difference ($I(t)_{ON} - I(t)_{OFF}$) and the ratio ($I(t)_{ON}/I(t)_{OFF}$) profiles, together with $I(t)_{OFF}$. The results are given in Table S1 of the SI. The difference of $I(t)_{ON} - I(t)_{OFF}$ corresponds to the time-resolved decay of E-PL signals taken at the second harmonic of the modulation frequency.

The average lifetimes (τ_{ave}) given by $\tau_{ave} = \sum_{i=1}^{3} A_i\tau_i / \sum_{i=1}^{3} A_i$ obtained from $I(t)_{ON}$ and $I(t)_{OFF}$ are also shown in Table S1. The lifetime becomes longer in the presence of **F** at both bands G1 and G2 in both of the samples. The difference between decay profiles observed with **F** and at zero field is always positive (Figures 8 and 9), indicating that the PL intensity is enhanced by **F**. This result is consistent with the steady-state E-PL spectra taken at the second harmonic of the modulation

DOI: 10.1021/acsaem.8b01171
ACS Appl. Energy Mater. 2018, 1, 6136−6151

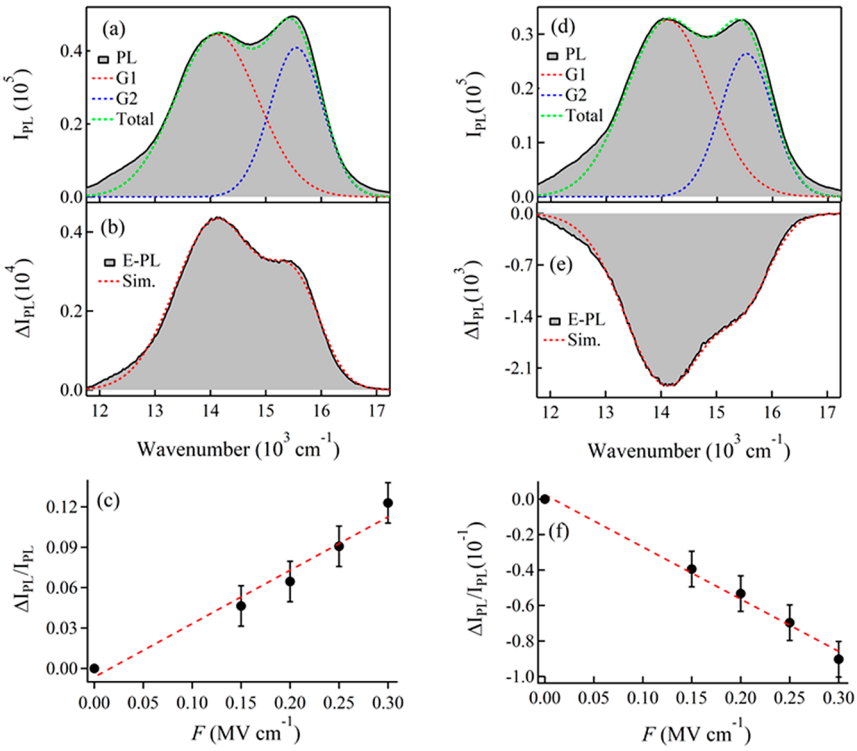

Figure 7. (a, d) PL spectra of sample II and its decomposition to the bands G1 and G2 having a Gaussian profile. (b, e) E-PL spectra observed with the first harmonic of the modulation frequency of the applied field having a strength of 0.3 MV cm^{-1} with a positive direction (b) and negative direction (e) and the simulated E-PL spectra (red dotted line) as a sum of the G1 and G2 bands. (c, f) Plots of $\Delta I_{PL}/I_{PL}$ as a function of the applied electric field strength. In the plots, the maximum intensity of G1 of the E-PL spectra was monitored. PL and E-PL spectra were simultaneously measured. The spectra observed with a field having the negative direction was measured following the measurements with a field having the positive direction.

Table 2. $\Delta I_{PL}/I_{PL}$ for G1 and G2 of Samples I and II Determined from the E-PL Spectra Observed at the First Harmonic of the Modulation Frequency of F and the PL Spectra Observed Simultaneously[a]

	F = +0.3 MV cm^{-1}		F = −0.3 MV cm^{-1}	
	G1 band	G2 band	G1 band	G2 band
sample I	0.10	0.08	− 0.08	− 0.06
sample II	0.12	0.07	− 0.09	− 0.05

[a]The applied field strength was 0.3 MV cm^{-1}. The positive and negative signs in the field strength represent the field direction; i.e., the positive and negative signs correspond to the positive and negative directions, respectively. See the text for details. Note that ΔI_{PL} is linearly proportional to the strength of the applied electric field.

frequency of **F**, where the field-induced increase of the PL intensity was observed (Figure 5). The magnitude of the pre-exponential factor A_i corresponds to the population of the emitting state. The ratio of A_i at 0.3 MV cm^{-1} to that at zero field is very close to unity at t = 0 for both G1 and G2 (Figures 8d,h and 9d,h), showing that the initial population of the emitting state is unaffected by **F**, in the quadratic field effect. On the other hand, the ratio becomes larger with increasing time, t, in both samples, indicating that the average lifetime becomes longer in the presence of **F** (Table S1). The field-induced increase of PL lifetime observed at the second harmonic of the modulation frequency leads to a conclusion that the enhancement of PL intensity induced as the quadratic field effect is due to the field-induced de-enhancement of nonradiative relaxation process at the emitting state of PL in both of the samples. As mentioned already, field-induced change in the zeroth derivative component, i.e., A_χ in eq 1 is as small as the order of 10^{-5}. Note that the magnitude of E-PL was in the order of 10^{-2} (see Table 1), which is 3 orders of magnitude larger than that of A_χ, indicating that the field-induced change in radiative decay rate at the PL emitting state is negligibly small.

The analyses described above were done for $I(t)_{ON}$ = CH1 + CH3 and $I(t)_{OFF}$ = CH2 + CH4. These analyses reveal the electric field effects on the decay processes that are averaged over the different field directions on the P3HT film. By measuring the E-PL spectra at the fundamental frequency of the modulating applied electric field, we observed a marked difference between the E-PL spectra taken at the opposite field directions, as shown in Figures 6 and 7. Further information, i.e., electric field effects on the decay dynamics under the opposite field directions, can be obtained by analyzing the decay curves of CH1 and CH3 separately. As already mentioned, the decay profiles observed in the presence of **F** of +0.3, −0.3, and 0 MV cm^{-1} correspond to CH1, CH3, and (CH2 + CH4)/2, respectively. The ratio between the decay profile stored in CH2 and that in CH4, both of which are considered to have been taken in the absence of ***F***, was unity over the full decay (see Figures S9 and S10 of the SI), indicating the reliability both of the operation of the instruments and of the analysis. Then, PL decay profiles of (CH2 + CH4)/2 can be regarded as the average decay profile at zero field without any doubt.

The decay profiles of CH1 and CH3 observed for sample I monitored at 640 and 705 nm and the simulated ones are

DOI: 10.1021/acsaem.8b01171
ACS Appl. Energy Mater. 2018, 1, 6136−6151

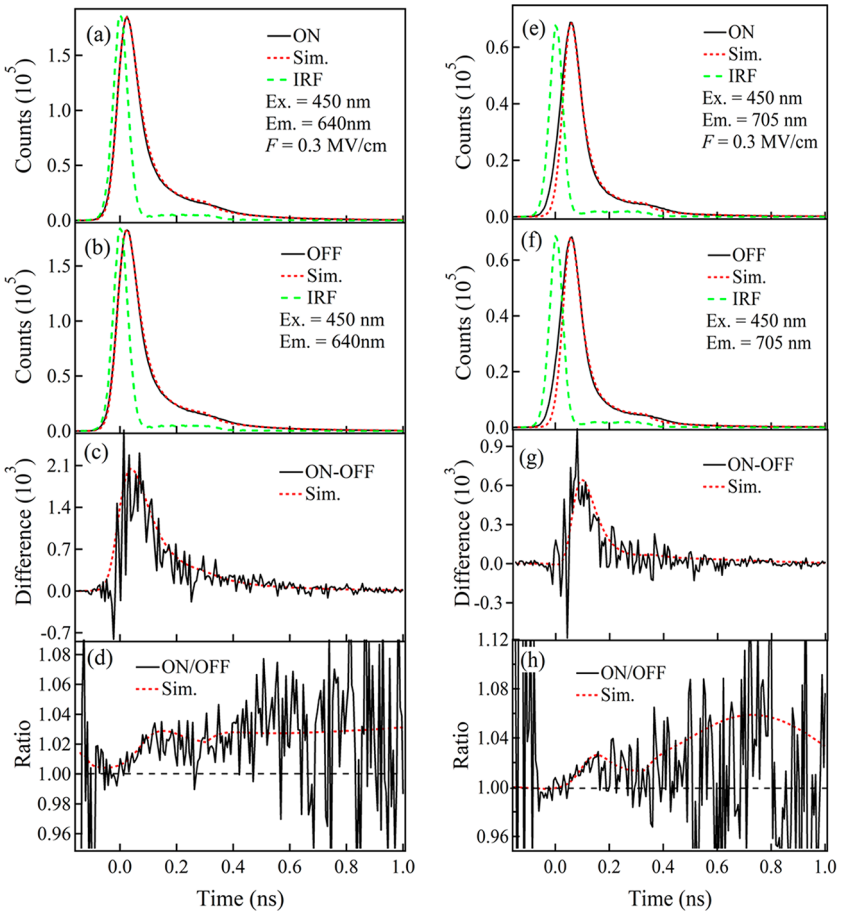

Figure 8. PL decay profiles of sample I. (a, e) Decay profile observed at 0.3 MV cm^{-1} (black line), simulated curve (red line), and instrument response function (green), (b, f) decay profile observed at zero field (black line), simulated curve (red line), and instrument response function (green), (c, g) difference between the two decay profiles at zero field and at 0.3 MVcm^{-1}, i.e., $I(t)_{ON} - I(t)_{OFF}$ (black line) and simulated curve (red line), and (d, h) ratio between the two decay profiles, i.e., $I(t)_{ON}/I(t)_{OFF}$ (black line) and simulated curve (red line). The results in the left and right columns were obtained, respectively, by monitoring PL at 640 and 705 nm. The decay at zero field was obtained from CH2 + CH4, while the decay at 0.3 MV cm^{-1} was obtained from CH1 + CH3. See the text for the detail.

shown in Figures S5 and 6 of the SI. Similar results were observed for sample II, as shown in Figures S7 and S8 of the SI. In these figures, the difference and ratio between the decay profile of CH1 or CH3 and (CH2 + CH4)/2 are also shown. The lifetime and pre-exponential factor for each decaying component of the decays obtained with a field strength of +0.3 MV cm^{-1} (CH1), 0 [(CH2 + CH4)/2], and −0.3 MV cm^{-1} (CH3) were determined from the simulation of the observed decay profiles, their difference and ratio (see Table S2 of SI). CH1 and CH3 involve both the linear and quadratic field effects on decay profiles, while CH1 + CH3 shows only the quadratic field effect because the linear field effect gets balanced out. Therefore, CH1 − (CH1 + CH3)/2 (resulting in (CH1 − CH3)/2)) and CH3 − (CH1 + CH3)/2 (resulting in (CH3 − CH1)/2)) involve only the linear field effect because the quadratic field effect is subtracted. In order to extract the linear field effect from the observed decay profiles, therefore, (CH1 − CH3)/2 as well as [(CH1 − CH3)/2]/[(CH2 + CH4)/2] and [(CH3 − CH1)/2]/[(CH2 + CH4)/2] were obtained for G1 and G2 of both of the samples. The results are shown in Figures 10 and 11 for samples I and II, respectively.

As shown in Figures S5b, S6b, S7b, and S8b of the SI, the difference between the decay profiles at +0.3 MV cm^{-1} and at zero field, i.e., [CH1 − (CH2 + CH4)/2] was positive. These results indicate the field-induced enhancement of PL intensity with the positive field direction, as the linear field effect, which is consistent with the E-PL spectrum observed at the first harmonic of the modulation frequency of **F** having the positive direction (Figures 6b and 7b). When the direction of the electric field was reversed, the difference between the decay profiles at −0.3 MV cm^{-1} and the zero field, i.e., [CH3 − (CH2 + CH4)/2] was negative in the whole time region (see Figures S5e, S6e, S7e, and S8e of the SI), indicating the field-induced quenching of PL with the negative field direction, as a linear field effect. This is also consistent with the E-PL spectrum observed at the first harmonic of the modulation frequency of **F** having the negative direction (Figures 6e and 7e).

As shown in Table S2, the sum of the pre-exponential factors, i.e., $\sum_{i=1}^{3} A_i$, at +0.3 MV cm^{-1} is a little larger than that at zero field for G2 in both samples I and II. On the other hand, this value at −0.3 MV cm^{-1} is a little smaller than that at zero field for G2 in both samples. These results show that the sum of the pre-exponential factors of decaying components of G2 becomes larger and smaller with the applied electric field, respectively, depending on the applied field direction. In other words, the population of the PL emitting state of the G2 band following photoexcitation increases and decreases, respectively, as the external electric field is applied in the positive and

DOI: 10.1021/acsaem.8b01171
ACS Appl. Energy Mater. 2018, 1, 6136−6151

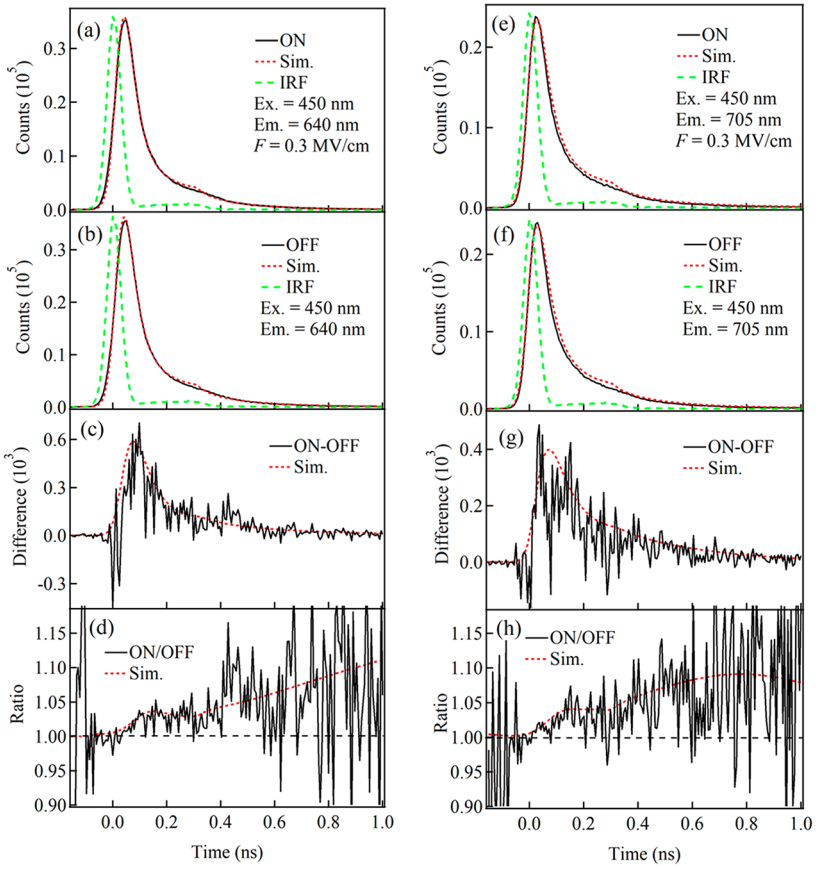

Figure 9. PL decay profiles of sample II. (a, e) Decay profile observed at 0.3 MV cm^{-1} (black line), simulated curve (red line), and instrument response function (green), (b, f) decay profile observed at zero field (black line), simulated curve (red line), and instrument response function (green), (c, g) difference between the two decay profiles at zero field and at 0.3 $MVcm^{-1}$, i.e., $I(t)_{ON} - I(t)_{OFF}$ (black line) and simulated curve (red line), and (d, h) ratio between the two decay profiles, i.e., $I(t)_{ON}/I(t)_{OFF}$ (black line) and simulated curve (red line). The results in the left and right columns were obtained, respectively, by monitoring PL at 640 and 705 nm. The decay at zero field was obtained from CH2 + CH4, while the decay at 0.3 MV cm^{-1} was obtained from CH1 + CH3. See the text for the detail.

negative directions. In the decay profiles, the ratio of CH1/(CH2 + CH4)/2 at $t = 0$ is larger than unity for G2 (Figures S5c and S7c of the SI), and CH1 − CH3 for G2 shows a nonzero positive value at $t = 0$ (see Figures 10c and 11c). On the other hand, the ratio of CH3/(CH2 + CH4)/2 at $t = 0$ is smaller than unity (Figures S5f and S7f of the SI), and CH3 − CH1 shows nonzero negative value at $t = 0$ for G2 (Figures 10d and 11d). Thus, it is clearly known that the population of the PL emitting state of G2 is affected by **F**, as the linear field effect. Regarding the emitting state of G1, CH1/(CH2 + CH4)/2 and CH3/(CH2 + CH4)/2 are nearly unity at $t = 0$ (Figures S6c,f and S8c,f of the SI), and CH1 − CH3 is nearly zero at $t = 0$ (Figures 10g,h and 11g,h), indicating that the population of the emitting state of G1 following photoexcitation is not affected by applied electric fields in both samples, in contrast with G2.

Field-induced change in PL lifetime caused by the linear field effect can be also confirmed. The time profiles of (CH1 − CH3)/(CH2 + CH4) and (CH3 − CH1)/(CH2 + CH4) of sample I given in Figure 10c,d for G2 and Figure 10g,h for G1 show monotonic increases and decreases, respectively, as a function of time. These results clearly show that PL lifetime increases and decreases, respectively, for both G1 and G2 with application of **F** in the positive and negative directions, as a linear field effect. The same results were obtained for sample II, as shown in panels c,d and g,h of Figure 11. Thus, both the lifetime and pre-exponential factor of PL decays are affected by **F** in the G2 band, and only the lifetime is affected by **F** in the G1 band, as a linear field effect. We can then recognize the anisotropy in the field-induced change in decay parameters, which depend on the field direction.

DISCUSSION

The observed PL can be assigned to the fluorescence of P3HT, so the field effect on PL can be attributed to the field effects on the photochemical processes taking place in the P3HT film including the interfacial process, not on the dynamics of Sb_2S_3 film or mp-TiO_2 film.

The experimental results described in the previous section are summarized as follows: (1) As the quadratic electric field effect on PL, emission quantum yield (QY) increases in the presence of **F** for both G1 and G2. (2) As the linear field effect on PL, QY of PL increases and decreases in the presence of **F** with the positive and negative directions, respectively. (3) Lifetime elongation of the PL emitting state is the main cause of the quadratic field effect on PL intensity, that is, field-induced increase of the PL intensity. (4) Initial PL intensity following photoexcitation does not show the quadratic field effect, indicating the non-existence of the quadratic field effect in population of the PL emitting state following photoexcitation for both G1 and G2. (5) Time-resolved PL intensity of G2 at $t = 0$ increases and decreases with the positive and

DOI: 10.1021/acsaem.8b01171
ACS Appl. Energy Mater. 2018, 1, 6136−6151

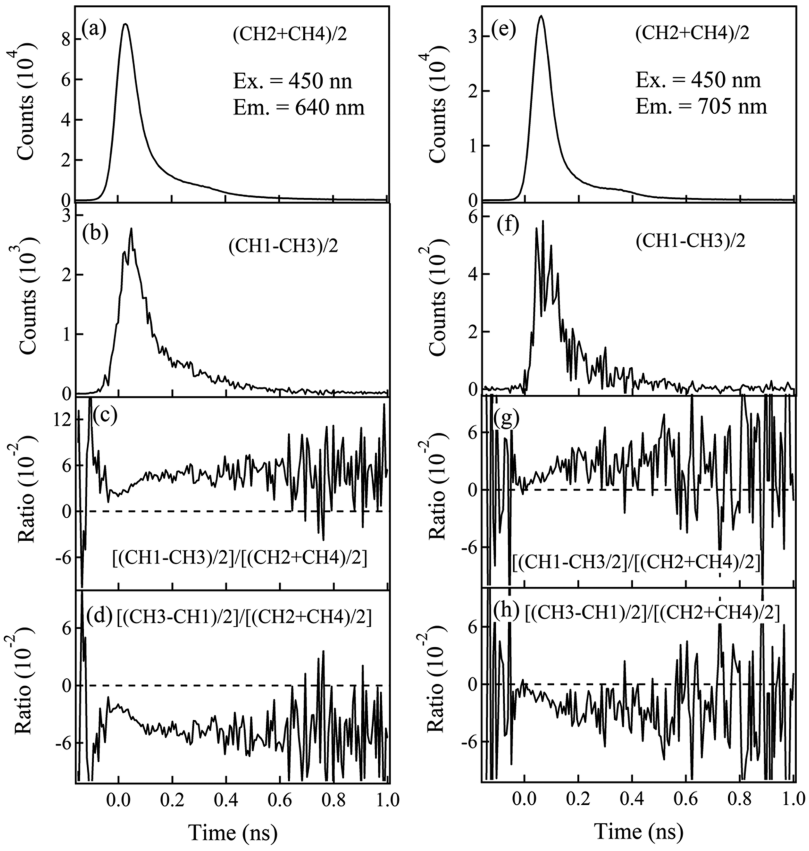

Figure 10. PL decay profiles of sample I monitored at 640 nm (left, a–d) and at 705 nm (right, e–h) and its field effect with 0.3 MV cm^{-1} where quadratic field effect is subtracted. (a, e) Decay profiles of (CH2 + CH4)/2 (decay at zero field), (b, f) decay profiles of (CH1 − CH3)/2, (c, g) decay profiles of (CH1 − CH3)/(CH2 + CH4) observed with positive field direction, and (d, h) decay profiles of (CH3 − CH1)/(CH2 + CH4) observed with negative field direction.

negative field directions, respectively, as the linear field effect. These field effects can be attributed to the field-induced increase and decrease in the population of the PL emitting state of G2 following photoexcitation. (6) In contrast with G2, the population of the emitting state of G1 is not affected by applied electric field even as a linear field effect. (7) PL lifetime becomes longer and shorter with the positive and negative field directions, respectively, as the linear field effect, in both G1 and G2 for both samples I and II.

The relaxation pathway following photoexcitation is schematically shown in Figure 12. Here, we consider two kinds of exciton states of P3HT: one is bound electron–hole pairs produced following photoexcitation, which corresponds to the Franck–Condon state and presently is called "hot exciton"; another is the state relaxed from hot exciton, which is called just "exciton".[55] The latter exciton may be also considered a kind of electron–hole pair. PL is considered to be emitted by the radiative recombination of electron–hole pairs, i.e., from exciton. Thus, the relaxation dynamics at the exciton includes radiative and nonradiative recombination processes of the charges, which are deactivation processes to the ground state. Another pathway is charge separation from hot excitons, which competes with the relaxation to the exciton (PL emitting state). It is considered that free electrons and holes are generated not only from hot exciton but also from the PL state (exciton) as a result of exciton dissociation. Since the PL emitting state is different from the photoexcited state, field-induced change of the pre-exponential factor at $t = 0$ is attributed to the field-induced change in population of the PL emitting state resulting from hot excitons. The increase of the PL lifetime observed as the quadratic field effect also suggests that the rate constant of the nonradiative process at the PL emitting states of both samples I and II decreases in the presence of **F**.

The average lifetime at zero field was 58 and 48 ps at 640 and 705 nm for mp-TiO_2/P3HT/PMMA, respectively, while the sample of mp-TiO_2/Sb_2S_3/P3HT/PMMA shows longer lifetimes of 62 and 76 ps, respectively (see Table S1 of the SI). There is a remarkable difference in PL lifetime especially at 705 nm (G1). Then, it is likely that photoluminescence comes not only from chromophores which are not in contact with an inorganic semiconductor but also from chromophores contacted with an inorganic semiconductor. We could observe the different electric field effects between the two emitting states (G1 and G2) which exist both in sample I and sample II. It is interesting to note that the intensity ratio between these different PL components depends on the interface with which P3HT makes contacts. As shown in the model in Figure 12, charge transfer of P3HT is considered to occur both from the photoexcited state (hot exciton) and from the relaxed state (exciton). Then, it should be stressed that the present results clearly indicate that hot exciton states of these two PL components show different behavior in dynamics as well as in electric field effect, i.e., both in charge transfer which competes with the relaxation to the cold exciton state and in its electric field effect, depending on the interface of P3HT.

As the quadratic field effect, both emissions of G1 and G2 show a similar behavior; PL quantum yield increases and

DOI: 10.1021/acsaem.8b01171
ACS Appl. Energy Mater. 2018, 1, 6136–6151

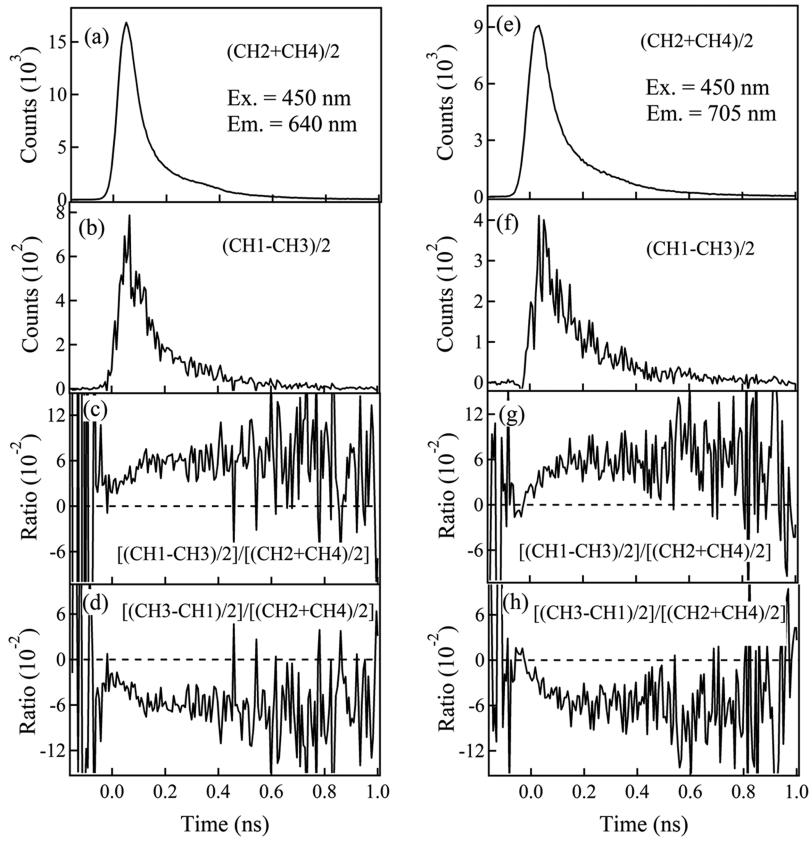

Figure 11. PL decay profiles of sample II monitored at 640 nm (left, a–d) and at 705 nm (right, e–h) and its field effect with 0.3 MV cm^{-1} where quadratic field effect is subtracted. (a, e) Decay profiles of (CH2 + CH4)/2 (decay at zero field), (b, f) decay profiles of (CH1 − CH3)/2, (c, g) decay profiles of (CH1 − CH3)/(CH2 + CH4) observed with positive field direction, and (d, h) decay profiles of (CH3 − CH1)/(CH2 + CH4) observed with negative field direction.

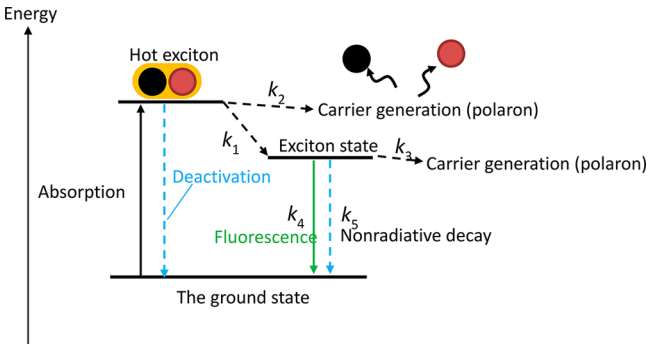

Figure 12. Schematic drawing of the relaxation pathway in P3HT films. The rate constants are indicated as k_1 and so on.

lifetime becomes longer in the presence of **F**, but no effect on initial population of the emitting state. As a linear field effect, on the other hand, G1 and G2 show different field effects from each other; the initial population of the emitting state of G2 increases and decreases in the presence of **F** with the positive and negative directions, respectively, whereas the initial population of G1 is not affected by application of electric field. Thus, the population of the emitting state is affected by electric field only for G2. These results indicate that the emitting states of G1 and G2 are generated from different hot exciton states from each other.

The fact that the G1 band is very different from the PL spectrum of P3HT in solution and that the G1 band is quite strong in sample II may indicate that the G1 band results from the hot excitons which are generated near the interface and strongly influenced by the materials contacting to P3HT, especially by the Sb_2S_3 film. The fact that the population of the emitting state of G1 is not affected by **F** may suggest that the dissociation of the hot excitons near the interface resulting in the production of free electrons and holes is inefficient probably because the relaxation of these hot excitons to the G1 emitting state is extremely fast. The efficient solar cell having a Sb_2S_3 layer may be related to the presence of the G1 emission which shows a longer PL lifetime, that is, a slow nonradiative process in the emitting state of the G1 band.[28] The binding energy of the exciton at the G1 emitting state may be much smaller than that at the G2 emitting state.

In contrast with the quadratic field effect, linear field effect which shows anisotropic behavior seems to give information about the interfacial problem. The energy level diagram of the multilayer films used in this work is shown in Figure S1 of the SI.[26,56−58] The PMMA layer is regarded as the hole blocking layer, because the level of the valence band is quite low. In order to explain the anisotropic behavior of the electric field effects on PL as well as carrier dynamics, the presence of an internal field may have to be considered in P3HT. The P3HT films show different fluorescence lifetimes from each other even at zero applied field in samples I and II, as shown in Tables S1 and S2 of the SI. In general, the built-in potential exists at the interface of different materials due to the difference of the Fermi energy level. The experimental verification of the internal field has also been reported for many multilayer film devices including P3HT−fullerene bulk

DOI: 10.1021/acsaem.8b01171
ACS Appl. Energy Mater. 2018, 1, 6136−6151

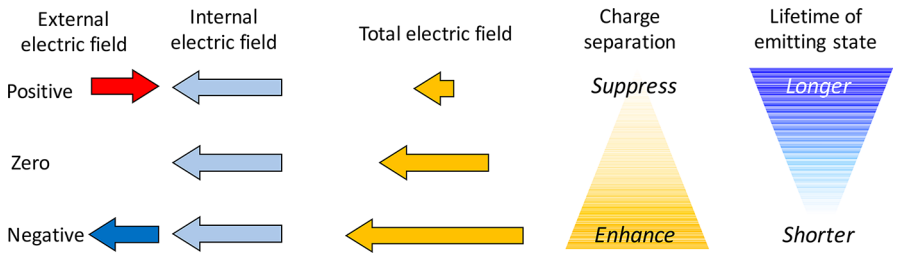

Figure 13. Schematic illustration of the variation of the total electric fields which result from the combination of the external electric fields with different directions and the internal electric fields. Both the extent of the exciton dissociation and the fluorescence lifetime of the emitting state are altered depending on the strength of the total electric field.

heterojunction photovoltaic cells.[59−61] We also observed the anisotropy in the carrier dynamics of ammonium lead halide perovskite semiconductor that arises from the internal field due to the built-in potential.[34]

The actual electric fields that are present in the P3HT film are given by the sum of the externally applied electric field and the internal electric field, if it exists. The internal field may point to the negative direction that is defined in Figure 1 and Figure S1 of the SI. The schematic illustration of the variation of the total electric fields which result from the different external field directions is given in Figure 13. The carrier dynamics may be affected by the internal electric field itself even when the external electric field is zero; dissociation of hot excitons (electron−hole pairs) produced following photoexcitation inside P3HT may be enhanced by internal fields. In the presence of **F** with the positive and negative directions, the total electric fields are considered to be weaker and stronger, respectively, than the internal electric field owing to the vector nature of the electric fields. To discuss the linear field effect on PL as well as on dynamics, therefore, the total electric field which depends on applied field direction may have to be taken into account.

We can explain the observed field-induced change in PL by the model shown in Figure 13. First, dissociation of hot excitons produced in the P3HT film, which competes with the relaxation to the emitting state of G2, is considered to be enhanced by electric fields. In fact, the separation to free electron and hole from exciton states is known to be promoted in the presence of the bias voltage in π-conjugated polymers.[30,46] The generation of free carriers from the hot excitons (denoted by k_2 in Figure 12) competes with the relaxation to the emitting state (denoted by k_1). Therefore, the decrease of the population of the emitting state is expected with the increase of the strength of the total electric field. In fact, initial population of the emitting state of G2 changes in the presence of F; increase or decrease of the population is induced by **F** having the positive or negative direction, respectively (Table S2). This result is consistently explained by the change in the yield of the dissociation of hot excitons into free carriers, which results from the change in strength of the total electric fields (Figure 13).

Field-induced elongation of the lifetime was confirmed not only as the quadratic field effect but also as the linear effect with the positive field direction. As already mentioned, the decay process from the emitting state can be divided into the radiative and nonradiative transitions. The E-A spectra show that the radiative rate constant to produce the fluorescence (k_4 in Figure 12) is little changed by **F**. The fluorescence lifetime of the emitting state gets shortened (lengthened) with the increase (decrease) of the nonradiative rate constant. The emitting state has a character of the charge separated state (electron−hole pair), so the nonradiative transition at the emitting state may be regarded as a kind of back-electron-transfer process. As shown in our previous work, photoinduced electron transfer as well as back-electron-transfer process is affected by electric field.[52,62,63] Then, it is likely that the observed field-induced change of the nonradiative decay (k_5 in Figure 12) from the emitting state in P3HT is related to the field-induced change in the back-electron-transfer process. We can explain the observations by assuming that the back-electron-transfer reaction is more enhanced by application of electric fields as a linear field effect. Even at zero external field, there is the effect of the internal electric field on the nonradiative transition rate constant k_5. When the external electric field **F** pointing to the positive direction is applied to the P3HT film, the strength of the total electric field becomes weaker than that of the internal electric field. Under this weaker field strength, the nonradiative rate constant k_5 becomes smaller, which results in the elongation of the fluorescence lifetime as well as in the increase of the population of the G2 emitting state, in comparison with that at zero external field. When the direction of the **F** is reversed, the strength of the total electric field becomes stronger, resulting in the shortening of the fluorescence lifetime for both G1 and G2 as well as the decrease of the population of the emitting state of G2, as the linear field effect. As mentioned above, it is likely that hot excitons produced near the interface between P3HT and TiO_2 or Sb_2S_3 relax to the G1 emitting state very efficiently, so the field effect on the population of the G1 emitting state is considered to be negligible. The fluorescence lifetime of the G1 emitting state shows an electric field effect similar to the one of the G2 emitting state. In contrast with the linear field effect, it is likely that the quadratic field effect induces the depression of the nonradiative rate at the PL emitting state for both G1 and G2.

■ CONCLUSION

External electric field effects on absorption and photoluminescence spectra, PL decays, and photoinduced dynamics of P3HT have been examined in multilayer films with heterojunction with TiO_2 or Sb_2S_3. The layered structures of the devices used in the present study were FTO/mp-TiO_2/P3HT/PMMA/Ag (sample I) and FTO/mp-TiO_2/Sb_2S_3/P3HT/PMMA/Ag (sample II). The electroabsorption spectra of P3HT observed in these samples are similar, and the magnitude of the change in electric dipole moment following absorption ($\Delta\mu$), which is characterized as a degree of the charge-transfer character in the Franck−Condon photoexcited state, was determined. The change in transition dipole moment

DOI: 10.1021/acsaem.8b01171
ACS Appl. Energy Mater. 2018, 1, 6136−6151

induced by externally applied electric field (**F**) was shown to be negligibly small.

The steady-state electrophotoluminescence spectra of the P3HT film were also measured both at the first harmonic and at the second harmonic of the modulation frequency of **F**. Field-induced increase both in intensity (quantum yield) and in lifetime observed at the second harmonic signal for both of the G1 and G2 bands indicate that the nonradiative decay rate at the PL emitting state is decelerated by application of electric field, as the quadratic field effect. Based on the measurements of the field-direction dependence of the E-PL spectra and decays, PL was shown to be enhanced by **F** with the positive direction for both G1 and G2, where positive electrode was connected to FTO and negative electrode was connected to silver. When the direction of **F** was reversed, field-induced PL quenching was observed, as a linear field effect.

PL decay profiles of P3HT were simulated by assuming a triexponential decay. The field-induced change both in the lifetime and in the pre-exponential factor of each decay component was determined. The increase of the PL intensity induced by the positive **F** mainly originates from the de-enhancement of the nonradiative decay process at the emitting state of P3HT for both G1 and G2. An increase of the population of the PL emitting state is also induced by **F** for G2. The field-induced quenching of PL of P3HT observed with the negative field direction was attributed to the field-induced enhancement of nonradiative decay rate at the emitting states of G1 and G2. Further, the field-induced decrease in population of the emitting state was observed for G2 emission with the negative field direction. The population of the emitting state of G1 was not affected by application of **F**. The emitting state of G1 may exist near the interface between P3HT and Sb_2S_3 or TiO_2, and the relaxation of hot excitons produced near the interface to the G1 emitting state seems to be so fast that the population of the emitting state of G1 may be not affected by application of electric field, in contrast with the G2 emission.

It is proposed that internal electric field exists in the P3HT layer, and the field-direction dependence on intensity and lifetime of PL may result from the synergy effect of external electric field and internal electric field. Depending on the direction of the **F**, the strength of the total electric field that is given by the sum of the **F** and the internal electric field also varies. The present results suggest that the strength of the total electric field increased and decreased, respectively, when **F** was applied in the negative direction and positive direction. Applied electric fields also induce the PL lifetime lengthening as a result of quadratic field effect, resulting from the field-induced depression of the nonradiative rate at the PL emitting state. The dissociation of hot excitons (electron−hole pairs) produced by photoexcitation is considered to be enhanced by electric field, resulting in the field-induced decrease of the population of the PL emitting state as well as field-induced quenching of PL. Then, it is considered that increase and decrease of the total electric field induce the enhancement and depression of the dissociation as well as the quenching and enhancement of PL by applied electric fields having the opposite field directions, respectively.

■ ASSOCIATED CONTENT

Supporting Information

The Supporting Information is available free of charge on the ACS Publications website at DOI: 10.1021/acsaem.8b01171.

Energy level diagram, sample preparation, details of the experimental setup of time-resolved E-PL measurements, field strength dependence of E-A signal, PL decay profile and time-resolved E-PL signal, PL lifetime parameters, and reference (PDF)

■ AUTHOR INFORMATION

Corresponding Author

*E-mail: nohta@nctu.edu.tw.

ORCID

Toshifumi Iimori: 0000-0003-2158-4378

Eric Wei-Guang Diau: 0000-0001-6113-5679

Nobuhiro Ohta: 0000-0003-4255-6448

Notes

The authors declare no competing financial interest.

■ ACKNOWLEDGMENTS

We thank Dr. Chin-Chun Chung for his help of the preparation of the sample including Sb_2S_3 film. Ministry of Science and Technology (MOST) in Taiwan provided financial support of this research (Grants MOST106-2811-M-009-018 and MOST107-3017-F009-003). This work was also financially supported by the Center for Emergent Functional Matter Science of National Chiao Tung University from The Featured Areas Research Center Program within the framework of the Higher Education Sprout Project by the Ministry of Education (MOE) in Taiwan.

■ REFERENCES

(1) Yu, G.; Gao, J.; Hummelen, J. C.; Wudl, F.; Heeger, A. J. Polymer Photovoltaic Cells: Enhanced Efficiencies via a Network of Internal Donor-Acceptor Heterojunctions. *Science* **1995**, *270*, 1789−1791.

(2) Günes, S.; Neugebauer, H.; Sariciftci, N. S. Conjugated Polymer-Based Organic Solar Cells. *Chem. Rev.* **2007**, *107*, 1324−1338.

(3) Cheng, Y.-J.; Yang, S.-H.; Hsu, C.-S. Synthesis of Conjugated Polymers for Organic Solar Cell Applications. *Chem. Rev.* **2009**, *109*, 5868−5923.

(4) Kang, H.; Lee, W.; Oh, J.; Kim, T.; Lee, C.; Kim, B. J. From Fullerene−Polymer to All-Polymer Solar Cells: The Importance of Molecular Packing, Orientation, and Morphology Control. *Acc. Chem. Res.* **2016**, *49*, 2424−2434.

(5) Kaloni, T. P.; Giesbrecht, P. K.; Schreckenbach, G.; Freund, M. S. Polythiophene: From Fundamental Perspectives to Applications. *Chem. Mater.* **2017**, *29*, 10248−10283.

(6) Yu, G.; Gao, J.; Hummelen, J. C.; Wudl, F.; Heeger, A. J. Polymer Photovoltaic Cells: Enhanced Efficiencies via a Network of Internal Donor-Acceptor Heterojunctions. *Science* **1995**, *270*, 1789−1791.

(7) Park, N.-G.; Grätzel, M.; Miyasaka, T.; Zhu, K.; Emery, K. Towards Stable and Commercially Available Perovskite Solar Cells. *Nat. Energy* **2016**, *1*, 16152.

(8) Grätzel, M. Dye-Sensitized Solar Cells. *J. Photochem. Photobiol., C* **2003**, *4*, 145−153.

(9) Nattestad, A.; Perera, I.; Spiccia, L. Developments in and Prospects for Photocathodic and Tandem Dye-Sensitized Solar Cells. *J. Photochem. Photobiol., C* **2016**, *28*, 44−71.

(10) Li, L. L.; Diau, E. W.-G. Porphyrin-Sensitized Solar Cells. *Chem. Soc. Rev.* **2013**, *42*, 291−304.

(11) Rhee, J. H.; Chung, C.-C.; Diau, E. W.-G. A Perspective of Mesoscopic Solar Cells Based on Metal Chalcogenide Quantum Dots and Organometal-Halide Perovskites. *NPG Asia Mater.* **2013**, *5*, e68.

(12) Kaiser, I.; Ernst, K.; Fischer, C. H.; Könenkamp, R.; Rost, C.; Sieber, I.; Lux-Steiner, M. C. The Eta-Solar Cell with $CuInS_2$: A

DOI: 10.1021/acsaem.8b01171
ACS Appl. Energy Mater. 2018, 1, 6136−6151

Photovoltaic Cell Concept Using an Extremely Thin Absorber (eta). *Sol. Energy Mater. Sol. Cells* **2001**, *67*, 89−96.
(13) Lévy-Clément, C.; Tena-Zaera, R.; Ryan, M. A.; Katty, A.; Hodes, G. CdSe-Sensitized p-CuSCN/Nanowire n-ZnO Heterojunctions. *Adv. Mater.* **2005**, *17*, 1512−1515.
(14) Belaidi, A.; Dittrich, T.; Kieven, D.; Tornow, J.; Schwarzburg, K.; Lux-Steiner, M. Influence of the Local Absorber Layer Thickness on the Performance of ZnO Nanorod Solar Cells. *Phys. Status Solidi RRL* **2008**, *2*, 172−174.
(15) Larramona, G.; Choné, C.; Jacob, A.; Sakakura, D.; Delatouche, B.; Péré, D.; Cieren, X.; Nagino, M.; Bayón, R. Nanostructured Photovoltaic Cell of the Type Titanium Dioxide, Cadmium Sulfide Thin Coating, and Copper Thiocyanate Showing High Quantum Efficiency. *Chem. Mater.* **2006**, *18*, 1688−1696.
(16) Itzhaik, Y.; Niitsoo, O.; Page, M.; Hodes, G. Sb_2S_3-Sensitized Nanoporous TiO_2 Solar Cells. *J. Phys. Chem. C* **2009**, *113*, 4254−4256.
(17) Nezu, S.; Larramona, G.; Choné, C.; Jacob, A.; Delatouche, B.; Péré, D.; Moisan, C. Light Soaking and Gas Effect on Nanocrystalline TiO_2/Sb_2S_3/CuSCN Photovoltaic Cells following Extremely Thin Absorber Concept. *J. Phys. Chem. C* **2010**, *114*, 6854−6859.
(18) Christians, J. A.; Leighton, D. T.; Kamat, P. V. Rate Limiting Interfacial Hole Transfer in Sb_2S_3 Solid-State Solar Cells. *Energy Environ. Sci.* **2014**, *7*, 1148−1158.
(19) Im, S. H.; Kim, H.-j.; Rhee, J. H.; Lim, C.-S.; Seok, S. I. Performance Improvement of Sb_2S_3-Sensitized Solar Cell by Introducing Hole Buffer Layer in Cobalt Complex electrolyte. *Energy Environ. Sci.* **2011**, *4*, 2799−2802.
(20) Kamruzzaman, M.; Chaoping, L.; Yishu, F.; Farid Ul Islam, A. K. M.; Zapien, J. A. Atmospheric Annealing Effect on TiO_2/Sb_2S_3/P3HT Heterojunction Hybrid Solar Cell Performance. *RSC Adv.* **2016**, *6*, 99282−99290.
(21) Kim, D.-H.; Lee, S.-J.; Park, M. S.; Kang, J.-K.; Heo, J. H.; Im, S. H.; Sung, S.-J. Highly Reproducible Planar Sb_2S_3-Sensitized Solar Cells Based on Atomic Layer Deposition. *Nanoscale* **2014**, *6*, 14549−14554.
(22) Lei, H.; Yang, G.; Guo, Y.; Xiong, L.; Qin, P.; Dai, X.; Zheng, X.; Ke, W.; Tao, H.; Chen, Z.; Li, B.; Fang, G. Efficient Planar Sb_2S_3 Solar Cells Using a Low-Temperature Solution-Processed Tin Oxide Electron Conductor. *Phys. Chem. Chem. Phys.* **2016**, *18*, 16436−16443.
(23) Lim, C.-S.; Im, S. H.; Chang, J. A.; Lee, Y. H.; Kim, H.-j.; Seok, S. I. Improvement of External Quantum Efficiency Depressed by Visible Light-Absorbing Hole Transport Material in Solid-State Semiconductor-Sensitized Heterojunction Solar Cells. *Nanoscale* **2012**, *4*, 429−432.
(24) O'Mahony, F. T. F.; Lutz, T.; Guijarro, N.; Gomez, R.; Haque, S. A. Electron and Hole Transfer at Metal Oxide/Sb_2S_3/Spiro-OMeTAD Heterojunctions. *Energy Environ. Sci.* **2012**, *5*, 9760−9764.
(25) Efstathiou, A.; Levin, E. R. Optical Properties of As_2Se_3, $(AsxSb_{1-x})_2Se_3$ and Sb_2S_3. *J. Opt. Soc. Am.* **1968**, *58*, 373−377.
(26) Lindblad, R.; Cappel, U. B.; O'Mahony, F. T.; Siegbahn, H.; Johansson, E. M.; Haque, S. A.; Rensmo, H. Energy Level Alignment in TiO_2/Metal Sulfide/Polymer Interfaces for Solar Cell Applications. *Phys. Chem. Chem. Phys.* **2014**, *16*, 17099−17107.
(27) Chung, C.-C.; Tsai, T.-W.; Wu, H.-P.; Diau, E. W.-G. Phosphonic Acid and Lithium Salt as Effective *p*-Dopants to Oxidize Spiro-OMeTAD for Mesoscopic Sb_2S_3 Solar Cells. *J. Phys. Chem. C* **2017**, *121*, 18472−18479.
(28) Chang, J. A.; Rhee, J. H.; Im, S. H.; Lee, Y. H.; Kim, H.-j.; Seok, S. I.; Nazeeruddin, M. K.; Gratzel, M. High-Performance Nanostructured Inorganic−Organic Heterojunction Solar Cells. *Nano Lett.* **2010**, *10*, 2609−2612.
(29) Cook, S.; Furube, A.; Katoh, R. Analysis of the Excited States of Regioregular Polythiophene P3HT. *Energy Environ. Sci.* **2008**, *1*, 294−299.
(30) Kersting, R.; Lemmer, U.; Deussen, M.; Bakker, H. J.; Mahrt, R. F.; Kurz, H.; Arkhipov, V. I.; Bässler, H.; Göbel, E. O. Ultrafast Field-Induced Dissociation of Excitons in Conjugated Polymers. *Phys. Rev. Lett.* **1994**, *73*, 1440−1443.
(31) Mehata, M. S.; Hsu, C.-S.; Lee, Y.-P.; Ohta, N. Electric-Field-Induced Enhancement/Quenching of Photoluminescence of π-Conjugated Polymer S3-PPV: Excitation Energy Dependence. *J. Phys. Chem. B* **2010**, *114*, 6258−6265.
(32) Kron, G.; Rau, U.; Werner, J. H. Influence of the Built-in Voltage on the Fill Factor of Dye-Sensitized Solar Cells. *J. Phys. Chem. B* **2003**, *107*, 13258−13261.
(33) Dong, C.; Li, X.; Zhao, W.; Jin, P.; Qi, J. Theoretical Analysis of Built-in Interfacial Electric Dipole Field in Dye-Sensitized Solar Cells. *J. Phys. Chem. C* **2013**, *117*, 9092−9103.
(34) Awasthi, K.; Wang, C.-Y.; Fathi, A.; Narra, S.; Diau, E. W.-G.; Ohta, N. Anisotropic Electric Field Effect on the Photoluminescence of $CH_3NH_3PbI_3$ Perovskite Sandwiched between Conducting and Insulating Films. *J. Phys. Chem. C* **2017**, *121*, 22700−22706.
(35) Boxer, S. G. Stark Realities. *J. Phys. Chem. B* **2009**, *113*, 2972−2983.
(36) Ohta, N. Electric-Field Effects on Photoinduced Dynamics and Function. *Pure Appl. Chem.* **2013**, *85*, 1427−1435.
(37) Chiang, H.-C.; Iimori, T.; Onodera, T.; Oikawa, H.; Ohta, N. Gigantic Electric Dipole Moment of Organic Microcrystals Evaluated in Dispersion Liquid with Polarized Electroabsorption Spectra. *J. Phys. Chem. C* **2012**, *116*, 8230−8235.
(38) Tayama, J.; Iimori, T.; Ohta, N. Comparative Study of Electroabsorption Spectra of Polar and Nonpolar Organic Molecules in Solution and in a Polymer Film. *J. Chem. Phys.* **2009**, *131*, 244509.
(39) Ohta, N. Electric Field Effects on Photochemical Dynamics in Solid Films. *Bull. Chem. Soc. Jpn.* **2002**, *75*, 1637−1655.
(40) Tsushima, M.; Ushizaka, T.; Ohta, N. Time-Resolved Measurement System of Electrofluorescence Spectra. *Rev. Sci. Instrum.* **2004**, *75*, 479−485.
(41) Liptay, W. Dipole Moments and Polarizabilities of Molecules in Excited Electronic States. In *Excited States*; Lim, E. C., Ed.; Academic Press: New York, 1974; Vol. *1*, p 129.
(42) Locknar, S. A.; Chowdhury, A.; Peteanu, L. A. Matrix and Temperature Effects on the Electronic Properties of Conjugated Molecules: An Electroabsorption Study of All-Trans-Retinal. *J. Phys. Chem. B* **2000**, *104*, 5816−5824.
(43) Jalviste, E.; Ohta, N. Theoretical Foundation of Electroabsorption Spectroscopy: Self-Contained Derivation of the Basic Equations with the Direction Cosine Method and the Euler Angle Method. *J. Photochem. Photobiol., C* **2007**, *8*, 30−46.
(44) Sakurai, K.; Tachibana, H.; Shiga, N.; Terakura, C.; Matsumoto, M.; Tokura, Y. Experimental Determination of Excitonic Structure in Polythiophene. *Phys. Rev. B: Condens. Matter Mater. Phys.* **1997**, *56*, 9552−9556.
(45) Liess, M.; Jeglinski, S.; Vardeny, Z. V.; Ozaki, M.; Yoshino, K.; Ding, Y.; Barton, T. Electroabsorption Spectroscopy of Luminescent and Nonluminescent π-Conjugated Polymers. *Phys. Rev. B: Condens. Matter Mater. Phys.* **1997**, *56*, 15712−15724.
(46) Liess, M.; Vardeny, Z. V.; Lane, P. A. Electromodulation of Charge-Transfer Photoexcitations in Pristine and C_{60}-Doped Conjugated Polymers. *Phys. Rev. B: Condens. Matter Mater. Phys.* **1999**, *59*, 11053−11061.
(47) Wachsmann-Hogiu, S.; Peteanu, L. A.; Liu, L. A.; Yaron, D. J.; Wildeman, J. The Effects of Structural and Microenvironmental Disorder on the Electronic Properties of Poly[2-methoxy,5-(2-ethylhexoxy)-1,4-phenylene vinylene] (MEH−PPV) and Related Oligomers. *J. Phys. Chem. B* **2003**, *107*, 5133−5143.
(48) Drori, T.; Holt, J.; Vardeny, Z. V. Optical Studies of the Charge Transfer Complex in Polythiophene/Fullerene Blends for Organic Photovoltaic Applications. *Phys. Rev. B: Condens. Matter Mater. Phys.* **2010**, *82*, 075207.
(49) Österbacka, R.; An, C. P.; Jiang, X. M.; Vardeny, Z. V. Two-Dimensional Electronic Excitations in Self-Assembled Conjugated Polymer Nanocrystals. *Science* **2000**, *287*, 839−842.
(50) Brown, P. J.; Sirringhaus, H.; Harrison, M.; Shkunov, M.; Friend, R. H. Optical Spectroscopy of Field-Induced Charge in Self-

DOI: 10.1021/acsaem.8b01171
ACS Appl. Energy Mater. 2018, 1, 6136−6151

Organized High Mobility Poly(3-hexylthiophene). *Phys. Rev. B: Condens. Matter Mater. Phys.* **2001**, *63*, 125204.
(51) Iimori, T.; Ito, R.; Ohta, N. Stark Spectroscopy of Rubrene. II. Stark Fluorescence Spectroscopy and Fluorescence Quenching Induced by an External Electric Field. *J. Phys. Chem. A* **2016**, *120*, 5497−5503.
(52) Iimori, T.; Yoshizawa, T.; Nakabayashi, T.; Ohta, N. Time-Resolved Measurements of the External Electric Field Effects on Fluorescence in Electron Donor and Acceptor Pairs of *N*-Ethylcarbazole and Dimethyl Terephthalate Doped in a Polymer Film. *Chem. Phys.* **2005**, *319*, 101−110.
(53) Brown, P. J.; Thomas, D. S.; Köhler, A.; Wilson, J. S.; Kim, J.-S.; Ramsdale, C. M.; Sirringhaus, H.; Friend, R. H. Effect of Interchain Interactions on the Absorption and Emission of Poly(3-hexylthiophene). *Phys. Rev. B: Condens. Matter Mater. Phys.* **2003**, *67*, 064203.
(54) Spano, F. C.; Silva, C. H- and J-Aggregate Behavior in Polymeric Semiconductors. *Annu. Rev. Phys. Chem.* **2014**, *65*, 477−500.
(55) Guo, J.; Ohkita, H.; Benten, H.; Ito, S. Near-IR Femtosecond Transient Absorption Spectroscopy of Ultrafast Polaron and Triplet Excitation Formation in Polythiophene Films with Different Regioregularities. *J. Am. Chem. Soc.* **2009**, *131*, 16869−16880.
(56) Takanezawa, K.; Tajima, K.; Hashimoto, K. Efficiency Enhancement of Polymer Photovoltaic Devices Hybridized with ZnO Nanorod Arrays by the Introduction of a Vanadium Oxide Buffer Layer. *Appl. Phys. Lett.* **2008**, *93*, 063308.
(57) Versavel, M. Y.; Haber, J. A. Structural and Optical Properties of Amorphous and Crystalline Antimony Sulfide Thin-Films. *Thin Solid Films* **2007**, *515*, 7171−7176.
(58) Wu, C.; Li, F.; Guo, T. Efficient Tristable Resistive Memory Based on Single Layer Graphene/Insulating Polymer Multi-Stacking Layer. *Appl. Phys. Lett.* **2014**, *104*, 183105.
(59) Kniepert, J.; Schubert, M.; Blakesley, J. C.; Neher, D. Photogeneration and Recombination in P3HT/PCBM Solar Cells Probed by Time-Delayed Collection Field Experiments. *J. Phys. Chem. Lett.* **2011**, *2*, 700−705.
(60) Mingebach, M.; Deibel, C.; Dyakonov, V. Built-In Potential and Validity of the Mott-Schottky Analysis in Organic Bulk Heterojunction Solar Cells. *Phys. Rev. B: Condens. Matter Mater. Phys.* **2011**, *84*, 153201.
(61) Kemerink, M.; Kramer, J. M.; Gommans, H. H. P.; Janssen, R. A. J. Temperature-Dependent Built-In Potential in Organic Semiconductor Devices. *Appl. Phys. Lett.* **2006**, *88*, 192108.
(62) Wahadoszamen, M.; Nakabayashi, T.; Kang, S.; Imahori, H.; Ohta, N. External Electric Field Effects on Absorption and Fluorescence Spectra of a Fullerene Derivative and Its Mixture with Zinc-Tetraphenylporphyrin Doped in a PMMA Film. *J. Phys. Chem. B* **2006**, *110*, 20354−20361.
(63) Yoshizawa, T.; Mizoguchi, M.; Iimori, T.; Nakabayashi, T.; Ohta, N. Effects of Electric and Magnetic Fields on Fluorescence in Electron Donor and Acceptor Pairs of Pyrene and *N*-Methylphthalimide Doped in a Polymer Film. *Chem. Phys.* **2006**, *324*, 26−39.

DOI: 10.1021/acsaem.8b01171
ACS Appl. Energy Mater. 2018, 1, 6136−6151